J. Fluid Mech. (2002), *vol.* 453, *pp.* 21–38.
DOI: 10.1017/S0022112001006590 Printed in the United Kingdom

Ferromagnetic rotating Couette flow: the role of magnetic viscosity

By J. E. HART

Program in Atmospheric and Oceanic Sciences, University of Colorado, Boulder, CO 80302, USA

(Received 21 February 2001 and in revised form 19 July 2001)

A theory is constructed for rotating plane Couette flow of ferrofluid that is subject to the field generated by a periodic array of magnets. The system that is analysed contains a substantial lateral magnetic buoyancy, or magnetic gravity, allowing the configuration to be used in experimental studies of stratified shear flows in a connected geometry.

However, the spatial variation of the magnetic vector field of the magnet stack leads to magnetically generated wavy flows via the action of flow vorticity on the particle orientation in the suspension. The basic rotating Couette flow instabilities may also be affected by the same mechanism, which is sometimes referred to as rotational or 'magnetic viscosity'. Theoretical calculations show that the directly excited wavy flows are generally small, for anticipated experimental conditions, except when they resonate with the natural linear instabilities of the Couette flow. A weakly nonlinear analysis is carried out in order to predict the behaviour in these cases. Magnetic effects stabilize the fundamental roll instability of rotating Couette flow by about 10% for a typical laboratory realization.

1. Introduction

Taylor–Couette flow between differentially rotating cylinders, and the dynamically related problem of rotating channel flow, are classic configurations permitting comparisons of stability theory and experiments, studies of the transition to turbulence, and diagnoses of fully developed turbulence. Studies of these systems include Hart (1972), Johnston, Halleen & Lezius (1972), Tafti & Vanka (1991), Kristoffersen & Andersson (1993), Tagg (1994), and Piomelli & Liu (1995), amongst many others. A natural and desirable extension to these experiments is the addition of a density stratification and a gravitational buoyancy force that are perpendicular to the vertical walls and to the imposed vertical rotation vector. Such a physical arrangement would permit valuable observations of instability, transition, and turbulence in stratified shear flows. For example, we could study thermal convection in the presence of 'vertical' shear, a problem treated theoretically by Matthews & Cox (1997). Alternatively, it would be possible to investigate the effects of radial buoyancy on the stationary axisymmetric and the propagating non-axisymmetric instabilities of the Taylor–Couette system. Such studies would have many applications, from basic engineering to geophysical and astrophysical problems.

However, it is not easy to generate a 'radial gravity' in the Taylor–Couette geometry, or to produce a horizontal 'lateral gravity' in the case of a channel flow rotating about its vertical axis. In the former situation, very rapid rotation of both the inner and outer cylinders can lead to a dynamically significant radially directed centrifugal buoyancy

force. The linear instability theory for this problem, in the thermally unstable case with the outer wall heated, has been studied by Kropp & Busse (1991). However, only a small segment of the usually accessible Ω_i/Ω_o parameter plane can be addressed using this method. The two rotation rates must be large and nearly equal, so the motions necessarily will have small Rossby number and will be strongly constrained by rotation.

Hart, Glatzmaier & Toomre (1986) used dielectric polarization forces in a spherical capacitor to study thermal convection in a rotating hemispherical shell with radial gravity. Both low and rapid rotation rates were studied. The apparatus had to be relatively small (radius ~ 3 cm, gap ~ 0.9 cm) in order that the electric field gradients (which decay as $1/r^3$) could be made large enough to give a large electrodynamic Rayleigh number. Ferrofluids have also been used to study geophysical problems experimentally, which particularly benefit from radial gravity. Ohlsen & Rhines (1997) looked at interfacial waves in a fluid held onto a sphere by centrally directed magnetic forces. The gravity used was relatively weak, and the whole system was placed in a neutral density two-fluid Plateau configuration, but the basic concepts of magnetic construction of radial buoyancy were demonstrated.

In a physical system that can attain both large Reynolds number and unit Richardson number, the artificial gravity must be large, and this requires a new experimental method. For example, consider a plane Couette flow in a gap of width D, with velocity U, which uses a low-viscosity organic oil (e.g. a 1 centistoke silicone oil) as a working fluid. In order to obtain a large value of $Re = UD/\nu$, with $Ri = g_l \alpha \Delta T D/U^2 = g_l \alpha \Delta T D^3/Re^2 \nu^2 \sim 1$, a substantial lateral (cross-channel) gravity g_l is required. Suppose the expansion coefficient, applied temperature contrast and gap width of the cell are given by $\alpha = 0.001\,^{\circ}\mathrm{C}^{-1}$, $\Delta T = 10\,^{\circ}\mathrm{C}$, $D = 0.02$ m, respectively. If we demand that $Re \sim 2000$, then g_l must be about $40\,\mathrm{m\,s^{-2}}$, or about 4 g. This paper outlines a conceptual design for a multi-g stratified shear flow experiment using a special arrangement of high-power magnets. The configuration discussed below leads to a large unidirectional magnetic gravity, but it also contains a highly structured spatially varying magnetic field. The interaction of such structured fields with vortical flows of ferrofluid has received little attention. In order to achieve a viable stratified shear flow experiment, it is desirable that so-called rotational viscosity (or 'magnetic viscosity') effects should not have a substantial impact on the basic flows and instabilities in the experiment.

Several authors have studied aspects of the Taylor–Couette instability in ferrofluid with relatively simple imposed magnetic fields. Niklas (1987) considers the stability of ferrofluid in the narrow-gap Taylor–Couette problem with a uniform axial field, a $1/r$ azimuthal field, or a $1/r$ radial field. The fields are considered uniform over the fluid-filled gap. The critical Taylor number is predicted to rise with Niklas's particular rotational viscosity parameter. The effect is not large, but may be observable under practical conditions. Stiles, Kagan & Hubbard (1987) similarly predict a small increase of Taylor number (up to 30%) with increasing magnetic field strength for a model cell with a uniform axial field. Measurements of inner cylinder torque in the presence of a modest axial field by Holderied, Schwab & Stierstadt (1988) suggest an increase of a few per cent in the critical inner cylinder rotation rate. Niklas, Muller-Krumbhaar & Lucke (1989) consider fields with a symmetry axis inclined to the axis of the Taylor–Couette cell. Stiles & Blennerhassett (1993) treat radial fields coupled with thermal gradients and find that magnetic buoyancy can destabilize the fluid. Their magnetic gravity effect was deemed small, and would normally be swamped by terrestrial gravity. Such destabilization might be seen in a microgravity environment.

The sorts of fields examined in these studies do not lead to strong radial magnetically induced buoyancy. Large-amplitude fields with axial and azimuthal symmetry are very difficult to implement across an apparatus of substantial size (so that the Reynolds number is large). The previous stability analyses did not consider any alteration to the classic $Ar+B/r$ basic state of Taylor–Couette flow by the interactions between the suspended particles, the basic flow shear, and the magnetic fields. Such changes will be absent if the applied field is axial and uniform. However, alterations to the classic mean flow are expected for many of the field distributions used in these studies, such as a radial $1/r$ field or an azimuthal $1/r$ field (Bashtovoy, Berkovsky & Vislovich 1988). The magnet-stack configuration considered here contains fields that vary substantially, even in a narrow gap. It is desirable to investigate the effects of these highly structured fields on basic flows and instabilities. In this paper, we investigate alterations to the basic state of plane rotating Couette flow when a spatially varying magnetic field is imposed on a channel filled with either weakly magnetized or magnetically saturated ferrofluid. In addition to modifying the basic state, the magnetic fields can also lead to changes in the critical points of linear instability because of magnetic forces acting on the unstable rolls themselves. These effects are estimated using perturbation theory. The formal statement of the problem is given in § 2. The linear analysis of § 3 shows that for most parameter settings and realistic experimental condition, the basic state changes should be small. However, resonances can arise when the magnetic viscosity terms force structures that excite the natural instability modes of the system. Section 4 outlines the nonlinear analysis that determines the expected corrections in resonant cases. Section 5 describes the magnetic viscosity effects on roll instabilities, and § 6 summarizes this study.

2. Formulation of the problem

For simplicity in analysis we consider a rectilinear geometry. The basic ideas apply to the Taylor–Couette problem, especially in the narrow-gap $\Omega_i/\Omega_o \sim 1$ approximation, when the results will carry over directly (Appendix B). As shown in figure 1, we consider a long channel, infinite in y, which is rotating about the vertical axis at rate Ω. The gap spacing is d and the ferrofluid is assumed to have Newtonian kinematic viscosity ν. Motion is driven in the contained ferrofluid by uniform longitudinal translation of the outer wall. This leads to a simple basic-state shear flow $u_b = Ux\hat{y}/d$. The key ingredient is a tall stack of rectangular bar magnets mounted to one side of the channel. The magnets are separated by non-magnetic spacers. In our idealized geometry, the bars are infinitely long in y. Each bar is magnetized with uniform magnetization $M_B\hat{z}$, directed vertically. In practice, neodymium–iron–boron magnets can have surface strengths approaching 1 tesla (10 000 gauss). The actual laboratory version will use cylindrical disk magnets, surrounded by a Taylor–Couette cell with variable speed inner and outer walls that can be maintained at different temperatures.

The equations of motion in the rotating frame of reference are, following Bashtovoy *et al.* (1988 ch. 6):

$$\partial \boldsymbol{u}/\partial t + \boldsymbol{u}\cdot\nabla\boldsymbol{u} + 2\boldsymbol{\Omega}\times\boldsymbol{u} - \nu\nabla^2\boldsymbol{u} + \frac{1}{\rho_0}\nabla p = \frac{\mu_0}{\rho_0}\boldsymbol{M}\cdot\nabla\boldsymbol{H} + \frac{\mu_0}{2\rho_0}\nabla\times(\boldsymbol{M}\times\boldsymbol{H}) \equiv \boldsymbol{a}_m, \quad (1a)$$

$$\nabla\cdot\boldsymbol{u} = 0, \quad (1b)$$

where $\boldsymbol{M}$ is the magnetization, $\boldsymbol{H}$ is the field intensity, μ_0 is the free-space permeability,

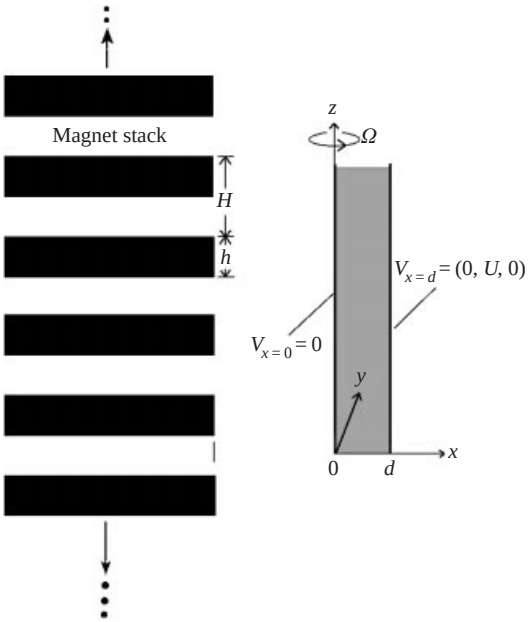

FIGURE 1. Cross-section of the model. A tall stack of bar magnets of height h and separation H (infinitely long in y) are set next to a vertical channel holding ferrofluid. Motion is driven by the uniform translation of the outer boundary. The system, including the magnets, rotates at rate Ω about the vertical axis.

and ρ_0 is the background density under the Boussinesq approximation where

$$\rho = \rho_0(1 - \alpha(T - T_0)).$$

The first magnetic term on the right-hand side of $(1a)$ is the normal term resulting from the divergence of the electromagnetic stress tensor. The second magnetic term arises when we include the coupling of the internal spin rate of particles in the ferrofluid to the fluid motion, along with conservation of internal angular momentum. We operate in the limit where the motion time scale is much longer than the very short ($< \mu$s) viscous relaxation time for the microscopic (~ 10 nm diameter) particles in the suspension. This formulation has been subject to various experimental tests, and is discussed in Rosensweig (1985), Hubbard & Stiles (1986), Niklas (1987), and many other references.

In the absence of relative motion, we expect the ferrofluid particles to align with the imposed field. The last term of $(1a)$ then vanishes. Suppose we want to construct the analogue of a lateral (or radial gravity). Operating well below the Curie point, the magnetization $\boldsymbol{M} \doteq \boldsymbol{M}_0\rho/\rho_0$, because variations in density (by fluctuations of temperature, for example) simply change the number of magnetite particles per unit volume in the suspension. A stratified shear flow configuration in the channel of figure 1 can be then attained if the 'magnetic buoyancy'

$$\boldsymbol{g}_l \alpha T \equiv \alpha T \left[\frac{\mu_0}{\rho_0}\boldsymbol{M} \cdot \nabla \boldsymbol{H}\right] \tag{2}$$

is large and horizontal. In principle, it would be useful to have $g_l \gg g$, both so that the Richardson number can be large, and so that the experiment can be carried out in the terrestrial laboratory.

The following reasoning shows that this appears relatively easy to do. The magnetic field is determined from the current-free Maxwell equations:

$$\nabla \cdot \boldsymbol{B} = 0, \quad \nabla \times \boldsymbol{H} = 0, \quad \boldsymbol{B} = \mu_0(\boldsymbol{H} + \boldsymbol{M}). \tag{3}$$

Since the saturation magnetization $\boldsymbol{M}$ of the ferrofluid is much less than $\boldsymbol{H}$, to lowest order we have

$$\nabla \cdot \boldsymbol{B} = \nabla \times \boldsymbol{B} = 0,$$

or

$$\boldsymbol{B} = -\nabla\varphi, \quad \nabla^2\varphi = 0. \tag{4}$$

Suppose the magnet stack is very tall compared with the height of the fluid channel. If it is infinitely high, the magnetic potential just to the right of the magnets (i.e. in the free space $x > -L_m$) can be written as

$$\varphi = \sum_{n=1}^{\infty} B_n \exp(-nk^* x) \sin(nk^* z)/nk^*, \tag{5}$$

where the origin of z is taken to be the zero plane for B_x, and $k^* \equiv 2\pi/H$ is the dimensional vertical wavenumber of the magnet stack. A (complicated) matching to the solution inside the stack, for $x \leqslant -L_m$, determines the coefficients. However, if the channel is far enough away from the stack, in its vicinity only the first term in the sum will be significant. Under these circumstances, the basic state magnetic field $\boldsymbol{B}_0$ is given by

$$\begin{aligned} \varphi &= B_1 \exp(-k^* x) \sin(k^* z)/k^*, \\ \boldsymbol{B}_0 &= [B_1 \exp(-k^* x) \sin(k^* z), 0 - B_1 \exp(-k^* x) \cos(k^* z)]. \end{aligned} \tag{6}$$

Here, B_1 is the measured (or calculated from the full problem) field amplitude at the left-hand wall of the channel. Figure 2 illustrates the field geometry. Although relatively complex in structure, compared with the field configurations used in previous studies, the magnitude of the field

$$B \equiv |\boldsymbol{B}_0| = B_1 \exp(-k^* x) \tag{7}$$

is very simple, and, as shown below, leads to a lateral gravity that can have the desired strength.

Figure 3 illustrates a numerical computation of the complete magnetostatic problem of the B-field due to the stack of 17 cylindrical magnets. Note the similarity of the contours of $B_{\hat{z}}$ with the model above. For $r > 1\,\text{cm}$, the field magnitude falls off almost exactly exponentially, with a uniform rate that corresponds to the vertical separation of the magnets. Detailed comparisons show good agreement between (6) and (7) and the medium-radius behaviour calculated numerically. At large radii, contributions from the dipole due to the finite stack height come into play, and the pure exponential decay is lost. When this happens, the magnetic body force, though conservative, is no longer purely horizontal. A similar effect occurs at distances closer to the magnet stack. The sum of two or more spatial modes of (5) no longer has a field magnitude that is unidirectional (i.e. it is now dependent on both x and z).

The lowest-order magnetization models for ferrofluid are taken to be:

$$\boldsymbol{M} = \boldsymbol{M}_w = \chi \boldsymbol{H} \tag{8a}$$

$$\boldsymbol{M} = \boldsymbol{M}_s = M_s \hat{H} \tag{8b}$$

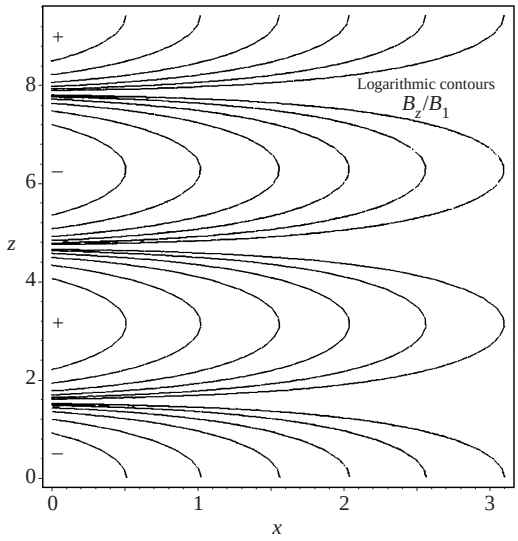

FIGURE 2. $B_{\hat{z}}$ distribution in the (x, z)-plane for the simple model (equation (6)).

These 'weak' and 'saturated' magnetization idealizations assume the suspended magnetite dipoles line up, to first approximation, with the applied field. Linear behaviour occurs in fields of order 0.1 tesla or smaller, while saturation can be achieved in fields of order 0.3 tesla or greater. Inserting these models into the right-hand side of (2) gives the magnetic buoyancy terms

$$\begin{aligned} \alpha T \mu_0 [\chi \nabla H^2]/\rho_0 &\approx \alpha T [\chi \nabla B^2]/\rho_0 = -2k^* \alpha T \chi B_1^2 \exp(-2k^* x)\hat{\boldsymbol{x}}/\rho_0, \\ \alpha T \mu_0 [M_s \nabla H]/\rho_0 &\approx \alpha T [M_s \nabla B]/\rho_0 = -k^* \alpha T M_s B_1 \exp(-k^* x)\hat{\boldsymbol{x}}/\rho_0, \end{aligned} \tag{9}$$

respectively. This is the basis for our experimental programme to construct a device with a strong radial (or lateral) buoyancy force. For powerful magnets, separated by $H \sim 10\,\mathrm{cm}$, and assuming that the ferrofluid is saturated, the lateral gravity is large. Taking $B_1 = 0.3t$ (3000 G), $M_s = 1.5 \times 10^4 \mathrm{A\,m^{-1}}$, $k^* = 60\,\mathrm{m^{-1}}$, $\rho_0 = 1200\,\mathrm{kg\,m^{-3}}$, we find $g_l \approx 20g$ at $x = 0$.

The magnetization formulae (equation (8)) are only a leading-order approximation. It has long been known that in the presence of a shear flow, the magnetic particles will twist out of line with $\boldsymbol{H}$. Shliomis (1972, 1974), proposed a model of this effect. We shall employ his relatively simple magnetization deviation formula that is valid in the limit where the motion time scale is long compared to the magnetization relaxation time. This is

$$\boldsymbol{M}' = \tau \frac{M_0}{2H_0} (\nabla \times \boldsymbol{u}) \times \boldsymbol{H}_0). \tag{10}$$

The magnetization and field intensity have been expanded according to $\boldsymbol{M} = \boldsymbol{M}_0 + \boldsymbol{M}'$, $\boldsymbol{H} = \boldsymbol{H}_0 + \boldsymbol{H}'$, where the primed fluctuations are assumed to be small compared with the basic states. The lowest-order magnetization is obtained from (8) with $\boldsymbol{H} = \boldsymbol{H}_0$, which is just $\boldsymbol{B}_0/\mu_0$. In obtaining (10) from the complete internal angular momentum balance and the full magnetization relaxation equation (as given in Niklas 1987, for example), $\boldsymbol{H}'$ is neglected under the rationale cited in Appendix A. The parameter

$$\tau \equiv \frac{\tau_b}{(1 + \tau_b \mu_0 M_0 H_0 / 6v\rho_0 \phi)} \equiv \frac{\tau_b}{(1 + a\tau_b \mu_0 M_0 H_0)} \tag{11}$$

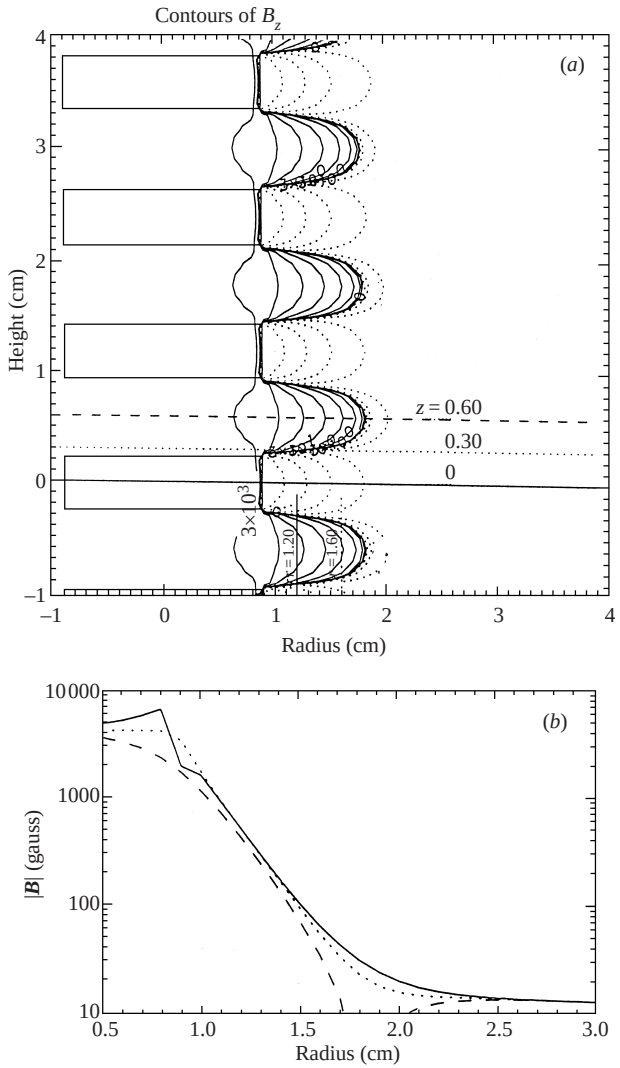

FIGURE 3. (*a*) Magnetic field $B_{\hat{z}}$ for a stack of 17 cylindrical disk magnets 0.48 cm high and 0.9 cm in radius, with $H = 1.2$ cm. Contours are logarithmic. (*b*) Magnitude of the field $|\boldsymbol{B}|$ *vs.* radius at $z = 0$ (the mid-plane of the stack).

is the modified magnetization decay time, where τ_b is the normal Brownian relaxation time ($\sim 10^{-6}$ s), and ϕ is the volume fraction of the suspension (typically 0.1–0.5). The computations are simplified if we consider $\tau \approx \tau_b = \text{constant}$. This assumption is solid for weak fields and (8*a*). The numbers for the strong gravity generation listed above, along with $\nu = 4 \times 10^{-6}\,\mathrm{m^2\,s^{-1}}$, give $a\tau_b\mu_0 M_0 H_0 \sim 0.4$ for a high-stress saturated case. Some effects of including this latter term are investigated below, but the more complicated parts of the analysis are simplified without it.

3. Linear analysis

The basic state for plane Couette flow is $\boldsymbol{u}_b = Ux\hat{\boldsymbol{y}}/d$. Using $\boldsymbol{H}_0 = \boldsymbol{B}_0/\mu_0$, along with (6) and (8), yields $\boldsymbol{M}_0$ from (8). Substitution into (10), and using the resulting

$\boldsymbol{M}'$ in the right-hand side of (1a) leads to the following magnetic acceleration terms that drive corrections to the basic state:

$$\boldsymbol{a}_m(\text{linear}(8a)) = -\frac{\tau\chi k^* U B_1^2}{4\mu_0 d}\exp(-2k^* x)\hat{\boldsymbol{y}}, \tag{12a}$$

$$\boldsymbol{a}_m(\text{saturated}(8b)) = -\frac{\tau k^* U M_s B_1}{8d}[\exp(-k^* x) + \exp(-k^* x)\cos(2k^* z)]\hat{\boldsymbol{y}}. \tag{12b}$$

In obtaining these results, it is again assumed that contributions from the magnetization correction $\boldsymbol{M}'$ dominate over those arising from the coupling of the magnetic field correction $\boldsymbol{H}'$ and the zeroeth-order magnetization $\boldsymbol{M}_0$. The basis for this is outlined in Appendix A. It is interesting that z-dependence only appears for the saturated magnetization model.

In all that follows we deal with non-dimensional equations, using U and d as velocity and length scales, respectively. The z-independent forcing terms in (12) serve to drive simple viscously balanced flows, solely in the y-direction, that are determined exactly (i.e. at any amplitude) from

$$\frac{\partial^2 V}{\partial^2 x} = \frac{d^2 a_m}{Uv}, \tag{13}$$

with $V(0) = V(1) = 0$. Once V is determined, the dynamic pressure correction is obtained from geostrophic balance. The results for linear and saturated magnetization are:

$$\left.\begin{aligned} V_{linear} &= C_{lin}[1 - x - \mathrm{e}^{-2kx} + x\mathrm{e}^{-2k}], \\ V_{sat} &= C_{sat}[1 - x - \mathrm{e}^{-kx} + x\mathrm{e}^{-k}], \end{aligned}\right\} \tag{14a}$$

where

$$\left.\begin{aligned} C_{lin} &= -\tau\chi B_1^2/16v\rho_0\mu_0 k, \\ C_{sat} &= -\tau M_s B_1/8v\rho_0 k, \end{aligned}\right\} \tag{14b}$$

and

$$k \equiv k^* d = 2\pi d/H \tag{15}$$

is the non-dimensional vertical wavenumber of the magnet stack.

Equation (13) is simple enough that the basic state corrections can be found without any approximation to τ. In this instance

$$a_m = \frac{-\tau_b M_s U k^* B_1 \mathrm{e}^{-kx}}{4d(1 + a^2 M_s^2 B_1^2 \mathrm{e}^{-2kx} + 8aM_s B_1 \mathrm{e}^{-kx})},$$

and

$$V_{sat\text{-}full\,\tau} = -C_{sat}\frac{\ln(aM_s B_1 + \mathrm{e}^{kx}) - \ln(\mathrm{e}^{kx}) - x\ln(aM_s B_1 + \mathrm{e}^{k}) + kx + (x-1)\ln(aM_s B_1 + 1)}{aM_s B_1}.$$

Figure 4(a) shows the profiles of V for the constant-τ case. Some numerical values illustrate the expected magnitude of these corrections. We set:

$$\begin{aligned} &d = 0.02\,\text{m}, \quad \tau_b = 10^{-6}\,\text{s}, \quad \chi = 0.01, \quad B_1 = 0.3\,\text{tesla}, \quad v = 5\times 10^{-6}\,\text{m}^2\,\text{s}^{-1}, \\ &M_s = 15\,000\,\text{A}\,\text{m}^{-1}, \quad \rho = 1200\,\text{kg}\,\text{m}^{-3}, \quad k = 2. \end{aligned} \tag{16}$$

These numbers reflect a workable configuration using quite strong neodynium–iron–boron magnets (nominal axial surface strength of order 3000 G) and a water-based

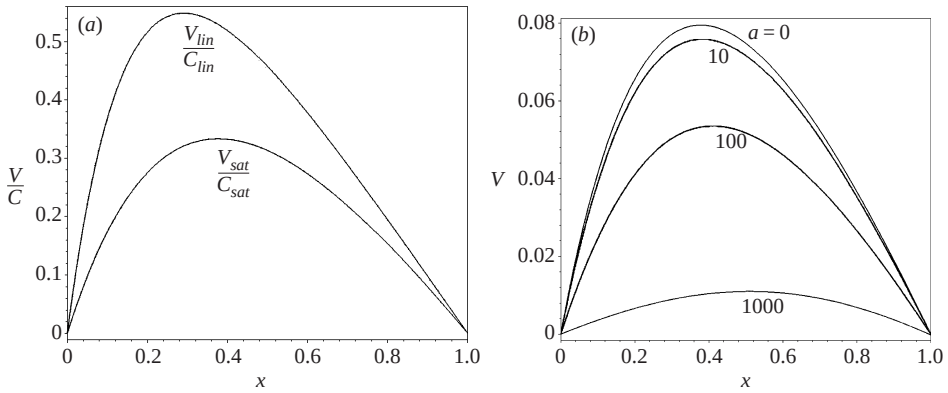

FIGURE 4. (*a*) The non-dimensional z-independent alteration to the basic flow $V(x)$, normalized by U) for both the saturated magnetization model, and the linear magnetization model. The non-dimensional magnet stack wavenumber $k = 2$ (see (15)). The amplitudes C_{lin} and C_{sat} are determined from equation (14*b*). (*b*) Effects of non-uniform τ (see (11)) on the saturated magnetization correction $V(x)$ calculated with numerical values given in (16).

ferrofluid with a saturation magnetization that is small enough that the viscosity is not too large (Rosensweig 1985 table 2.4). These parameter settings give $C_{lin} = -0.00375$, $C_{sat} = -0.0468$. As expected, the weak magnetization limit does not generate a significant basic-state alteration, but the high-field saturated case leads to about a 1.5% peak correction. The corrected flow is opposite to the basic linearly sheared current, but has no inflection points. For these same parameters, figure 4(*b*) shows the solution using the full expression for τ. Even though the size of a is not well known, its effect is to decrease the size of the modification to the basic current.

The above analysis shows that height-invariant corrections to the basic state are generated. These are similar to those calculated by Bashtovoy *et al.* (1998) for a hypothetical travelling-wave magnetic field, generated at a current sheet, that has a shape (when travelling with the wave) identical to that in (6). However, Bashtovoy *et al.* did not discuss the vertically wavy modes. Using the second term in (12*b*) as the forcing, the z-dependent steady two-dimensional problem is solved by assuming a small response (compared with U), and linearizing the equations of motion. We consider here only the stronger saturated-magnetization limit, where we must obtain the solution of

$$\nabla^6\psi + Q\psi_{zz} = \frac{Rod}{E^2U^2}a_{m\hat{y}_z} \equiv f_z, v_z = -E\nabla^2\psi. \tag{17}$$

Here,

$$f_z = \frac{\Lambda}{E}k^2\mathrm{e}^{-kx}\sin(2kz), \tag{18a}$$

$$u = \psi_z, \quad w = -\psi_x, \tag{18b}$$

$$\Gamma \equiv \frac{\tau M_s B_1}{4\nu\rho_0} = -2kC_{sat}, \tag{18c}$$

and

$$Q \equiv (1 + Ro)/E^2 = (1 + Ro)/Ta. \tag{19}$$

Ro is the Rossby number for the basic flow $U/2\Omega d$, and E is the Ekman number $\nu/2\Omega d^2$.

There is a direct analogy with the rigid-wall thermal convection problem. The PDE on the left-hand side of (17) is the same as that for two-dimensional steady convective roll instabilities, after exchanging the roles of x and z. Q is equivalent to the negative of the Rayleigh number. The boundary conditions are impermeable and no-slip: $\psi = \psi_x = \nabla^4\psi = 0$ at $x = 0, 1$. The solution is

$$\psi = -\frac{\Gamma \mathrm{e}^{-kx}\sin(2kz)}{27k^4 + 4Q} + \psi_h, \quad \psi_h = \phi(x)\sin(2kz). \tag{20}$$

The addition of the six homogeneous solutions, ψ_h, which have $\sin(2kz)$ vertical structure, is required to satisfy the boundary conditions. The solutions are found by symbolic manipulation (using MAPLE). The complex-exponential solutions are made up of six modes $a_j \exp(r_j x)$, with $(r^2 - 4k^2)^3 - 4k^2Q = 0$. The unknown coefficients a_j are found by applying the boundary conditions to (20). There is an apparent singularity if $Q = -27k^4/4$. However, the total solution is smooth across this point because the homogeneous solution has a shape there that is very close to the forced mode. It must be subtracted to satisfy $\psi(x = 0, 1) = 0$, say, rendering the total ψ finite at the singularity.

However, when $Q < 0$, the required free solution may be resonant. This happens whenever Q is an eigenvalue of the force-free version of (17) with modes proportional to $\exp(\mathrm{i}k'x)$ with $k' \equiv 2k$. For example, if $k' = 3.117$, that is for magnet wavenumber 1.5585, the linear solution fails if $Q = -1708$ (the critical Rayleigh number) since then the homogeneous solutions do not have enough degrees of freedom to satisfy all six boundary conditions. Mathematically, the determinant of the coefficients of the six non-homogeneous equations for the a_j terms vanishes whenever Q sits on the neutral curve for rigid boundary thermal convection problem (i.e. $Q = -Ra(k')$).

Figure 5 shows the magnitude of the response on the (k, Q)-plane. The magnitudes are relatively small, except along the neutral curve of thermal convection. The shape of the total x-dependent parts of (20) are illustrated in figure 6. As $-Q$ increases at fixed k', the homogeneous solutions correspond to higher cross-channel modes (equivalent to higher vertical modes in the thermal convection problem), and the total solution has more structure. Away from resonance, the peak correction to the basic flow is typically less than 1% of U. The z-dependent mean-flow corrections are weaker than the z-independent ones because of the extra effect of vertical viscous diffusion. Though in general relatively minor, these basic flow corrections could become significant for resonant conditions. We now proceed to remove the resonances using a weakly nonlinear expansion.

4. Weakly nonlinear results

First transform the variables using

$$\psi = \frac{E}{Ro}\Psi, \quad v = \frac{E^2}{Ro}V,$$

so that the nonlinear equations of steady two-dimensional motion become

$$\nabla^4\Psi + V_z = \partial\nabla^2\Psi/\partial t + J(\Psi, \nabla^2\Psi), \tag{21a}$$

$$\nabla^2 V - Q\Psi_z = \partial V/\partial t + J(\Psi, V) + \frac{Ro}{2E^2}\Gamma k \mathrm{e}^{-kx}\cos(2kz), \tag{21b}$$

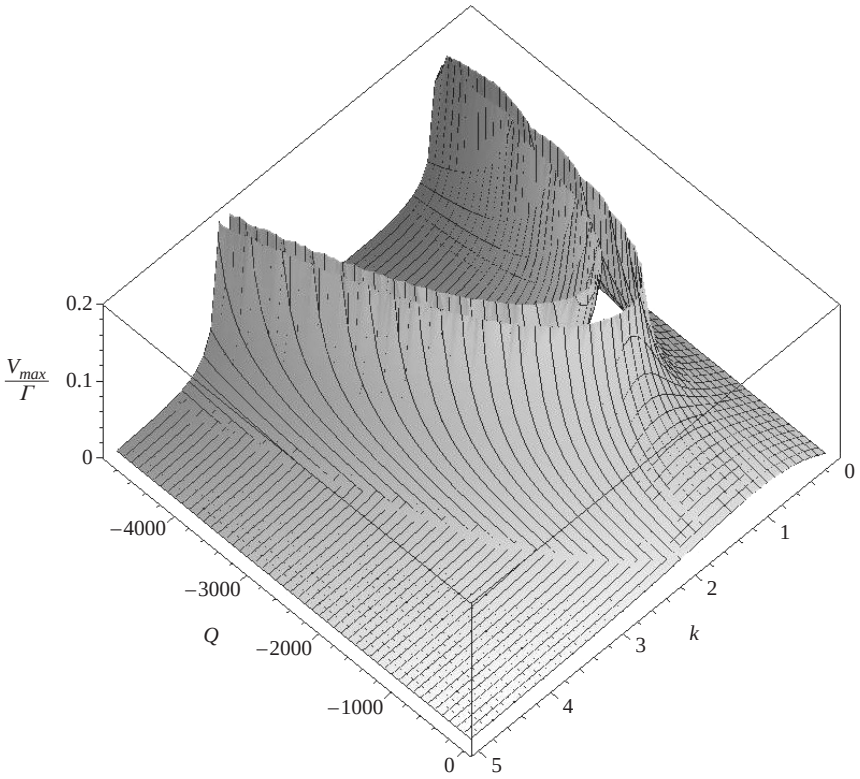

FIGURE 5. Linear response for the z-dependent forced modes with $\cos(2kz)$ vertical structure. The map shows the peak down-channel velocity, normalized by Γ.

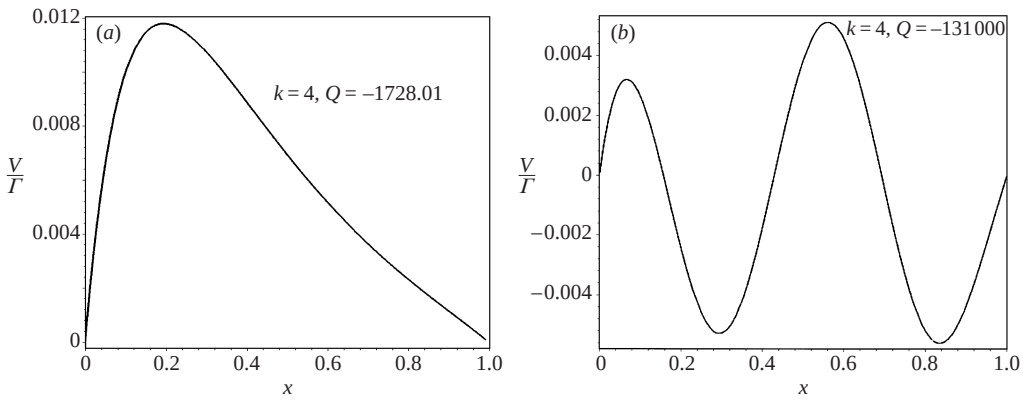

FIGURE 6. The x-dependent parts of the forced linear solutions for two situations: (a) nearly resonant forced solution; (b) large supercriticality where the free solution is a higher cross-channel mode.

where J is defined as the advection operator, e.g. $J(\Psi, V) \equiv \Psi_z V_x - \Psi_x V_z$. In the usual way we construct an amplitude expansion of form

$$\Psi = A\Psi_1 + A^2\Psi_2 + A^3\Psi_3 \ldots, \tag{22a}$$

$$V = AV_1 + A^2V_2 + A^3V_3 \ldots, \tag{22b}$$

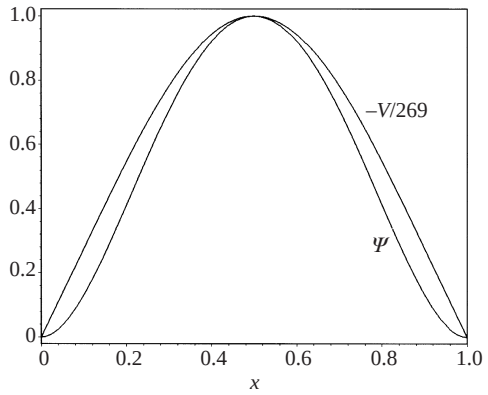

FIGURE 7. Linear eigenfunctions corresponding to $k' = 4$, $Q_C = -1880$.

where $\varepsilon \equiv (Q - Q_c)/Q_c \ll 1$, and Q_c is the rigid wall eigenvalue for a zero of the left-hand side of (21) for modes with wavenumber $k' \equiv 2k$. The small slow-time-varying amplitude $A(T \equiv |\varepsilon|t)$ is assumed to be of order $|\varepsilon|^{1/2}$. The forcing term on the extreme right-hand side of (21*b*) is assumed to be of order A^3.

The eigenfunction $\Psi_1 = \varphi_1(x)\sin(k'z)$, $V_1 = V_1(x)\cos(k'z)$, is found analytically from the homogeneous version of (21) obtained by omitting the right-hand sides. Figure 7 illustrates the eigenfunction for a typical case. These solutions are then iterated through the Jacobian operators to obtain the forced second-order problem. In contrast to the case with free boundaries, with rigid walls the vorticity advection in the fundamental roll mode does not vanish, and higher harmonics in z are excited. Although these have a small effect on the amplitude equation, it makes the calculation more tedious. Once Ψ_2 and V_2 are found, the solvability condition, in the form

$$\langle -Q_{c1}\Psi_1 L_{3\Psi} + V_1 L_{3V}\rangle = 0, \tag{23}$$

is applied. Here, the brackets denote an integration across the channel and over one wavelength of the perturbations vertically. L represents the forcing terms of the third-order problem:

$$L_{3\Psi} = |\varepsilon|\partial\nabla^2\Psi_1/\partial T + J(\Psi_1, \nabla^2\Psi_2) + J(\Psi_2, \nabla^2\Psi_1), \tag{24}$$

$$L_{3V} = |\varepsilon|\partial V_1/\partial T - \varepsilon Q_c \partial\Psi_1/\partial z + J(\Psi_1, V_2) + J(\Psi_2, V_1) + \frac{Ro}{2E^2}\Gamma k \mathrm{e}^{-kx}\cos(2kz), \tag{25}$$

where, T is the slow-time variable. The calculation again proceeds analytically via automated symbolic manipulation.

The resulting amplitude equation can be written in the form

$$c_0|\varepsilon|\mathrm{d}A(T)/\mathrm{d}T = -c_1\beta + c_2\varepsilon A - A^3, \tag{26}$$

where $\beta \equiv -\Gamma(Ro/E^2)$. β is positive because $Ro < -1$ for instability (which is required for resonance), and the c terms, as well as A, are real. The equilibration amplitude(s) may be more easily obtained by writing

$$A = (c_1\beta)^{1/3}\Lambda, \quad \gamma \equiv c_2\varepsilon/(c_1\beta)^{2/3}, \tag{27}$$

whence,

$$\Lambda^3 - \gamma\Lambda - 1 = 0. \tag{28}$$

This equation has multiple real roots if $\gamma > (\frac{27}{4})^{1/3} \sim 1.89$. In the case of multiple

k'	$-Q_c$	c_0	$10\,000\,c_1$	c_2
1	5854	0.747	3.11	6.39
2	2177	0.395	4.01	4.03
3	1711	0.285	3.63	3.61
3.117	1708	0.277	3.59	3.61
4	1879	0.231	2.72	3.68
5	2439	0.196	1.82	3.94
6	3418	0.169	1.16	4.29
7	4919	0.149	0.73	4.70
8	7085	0.133	0.46	5.15

TABLE 1. Terms in the amplitude equation (26).

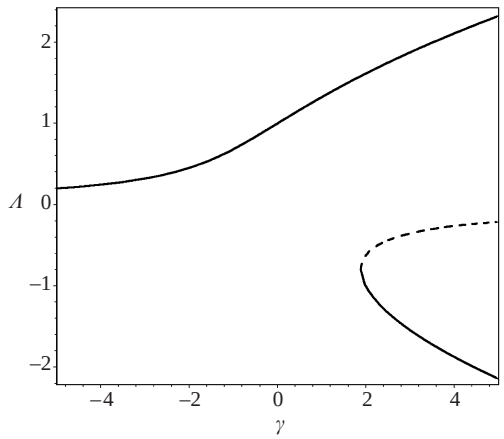

FIGURE 8. Stable branches of the equilibration equation (28).

roots, the two stable solutions have opposite signs and are the two largest (of the three) in magnitude. The solutions to (28) are illustrated in figure 8.

The mechanism that produces multiple states is simple. As ε increases, the two normal finite-amplitude instability modes, which are invariant to changes in the sign of A, become large and uncoupled from the interaction between the vorticity and the magnetic field. If ε (i.e. γ) is not large, the magnetic viscosity forcing will cause the negative finite-amplitude mode to be enhanced (and undergo an imperfect pitchfork bifurcation at $\varepsilon = 0$). At the same parameter settings, the positive amplitude mode is suppressed. This continues until the positive A mode has sufficient strength to overcome the negative magnetic effect, and we obtain two solutions at large enough γ. In practice, if $k' = 2k$ is much different from 3.117, the k' of lowest critical Q, in order to be in a subcritical regime with respect to this most unstable linear mode, ε will have to be large and negative. Under these circumstances there will be only one stable solution of the equilibration problem.

As an example, consider a situation with the parameter values given in (16), which has $k = 2$, or $k' = 4$. For an extreme case we take $\varepsilon = 0.35$. In addition, we must specify E. A large value is $E = 0.05$, which, under the conditions of (16), represents a slow rotation (a 600 s period). For this situation, $\gamma = 2.13$ and there are two stable solutions with a final peak amplitude for V of -0.118 or 0.079. That is, the distribution of V^*/U is given by these values multiplied by the structure function in

figure 7, multiplied by $\cos(2kz)$. When ε and E are smaller, there is typically only one solution. For example, if $E = 0.005$ (a 5 s period), and $\varepsilon = 0.1$, then $\gamma = 0.087$ and the peak amplitude is -0.0278. This last example has $Q_c = -1879$, and $Q = -2066$. The most unstable free mode (which has $Q_c = -1708$) sits at an effective supercriticality of $\varepsilon = 0.21$ at this parameter point. Using the above model, this free mode has an equilibrium amplitude $A = \sqrt{c_2}\varepsilon = 0.84$. Thus, the magnetically induced longitudinal rolls are small compared with the normal roll instability in the channel.

5. Effect of magnetic viscosity on instabilities

The above arguments show that the direct alterations to the basic state by non-Newtonian stresses, arising from the field of the magnet stack and the vorticity of the basic flow acting together on the particles in the ferrofluid, are not large. Such changes will not significantly alter the expected instabilities. However, the magnetization deviation is generated by the flow vorticity, and while the non-dimensional vorticity of the basic state is unity, that of roll instabilities is expected to be at least 20 or more, per unit amplitude. How do the magnetic forcing terms directly affect the linear instability? Anticipating that the corrections to the non-magnetic results will be small, and realizing that a full stability calculation will be complicated by non-constant-coefficient ODEs (because of the non-uniform magnetic field (6)) we approach the problem by perturbation expansion.

The linear stability equations can be written as

$$\nabla^4 \Psi' + \partial V'/\partial z = -Ro(\partial f_{\hat{x}}/\partial z - \partial f_{\hat{z}}/\partial x), \tag{29}$$

$$\nabla^2 V' - Q\partial \Psi'/\partial z = -Rof_{\hat{y}}/E, \tag{30}$$

where

$$\boldsymbol{f} = \frac{\tau MsU}{2\rho_0 d}\left\{[(\nabla \times \boldsymbol{u}') \times \hat{\boldsymbol{B}}_0] \cdot \nabla \boldsymbol{B}_0 + \tfrac{1}{2}\nabla \times [((\nabla \times \boldsymbol{u}') \times \hat{\boldsymbol{B}}_0) \times \boldsymbol{B}_0]\right\}, \tag{31}$$

with $u' = \Psi'_z/E$, and $w' = -\Psi'_x/E$. The saturation magnetization model (8b), to focus on the largest effects, and constant τ in the Shliomis model (10), to simplify the computation as much as is reasonable, have been used in (31).

The fields are expanded according to $\Psi' = \Psi'_1 + \delta\Psi'_2 + \ldots$, $V' = V'_1 + \delta V'_2 + \ldots$, with

$$\delta \equiv \frac{Q - Q_c}{Q_c} \ll 1. \tag{32}$$

At lowest order the usual linear stability problem without magnetics is recovered and Q_c is determined. An oscillatory vertical structure $\Psi' \propto \sin(k'(z + z_0))$ is assumed. The rigid-wall eigenfunctions are found analytically as in § 4. As Q is made more negative, the first longitudinal roll instability to be encountered has vertical wavenumber $k' = 3.117$ and $Q_c = -1708$. As this is the most unstable mode, we concentrate on finding only its change in stability. The computation of (31) is tedious, but fortunately it is only necessary to go to second order to find δ. This is because (31), when evaluated with the lowest-order velocities, projects onto the lowest-order instabilities, and therefore resonance removal at second order determines δ. $\boldsymbol{M}'$ involves vertical waves with wavenumber $\pm k' \pm k$, representing the composite of the roll instability and the periodicity of the magnet stack. When this is used in $\nabla \times (\boldsymbol{M}' \times \boldsymbol{B}_0)$, for example, wavenumbers $\pm k' \pm k \pm k$ enter the forcing of the second-order problem. Therefore, the second-order forcing has some components that project onto the vertical structure

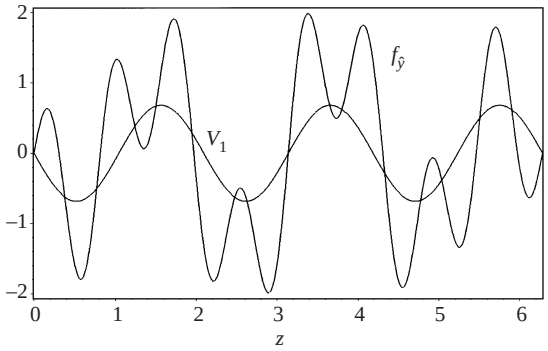

FIGURE 9. Vertical structure of the fundamental instability V and the second-order y-directed magnetic-deviation-induced forcing $f_{\hat{y}}$. $k' = 3$, $k = 2.5$, $Q = -1712$.

(wavenumber k') of the fundamental. This is illustrated in figure 9, which shows that there is a height integrated correlation between V_1 and $f_{\hat{y}}$. The result of the perturbation expansion is,

$$\delta = \frac{\langle Q_c Ro \Psi_1'[f_{\hat{x}z}(\Psi_1', V_1') - f_{\hat{z}x}(\Psi_1', V_1')] + V_1' Ro f_{\hat{y}}(\Psi_1', V_1')/E\rangle}{Q_c\langle V_1' \Psi_{1z}'\rangle} = c_3(k, k', Q_c)\frac{\tau M_S B_1}{\nu\rho_0}. \tag{33}$$

The brackets describe an average over x from 0 to 1, and over z from 0 to Z. The last limit, usually taken to be the vertical wavelength of the fundamental, $2\pi/k'$, is now the lowest vertical periodicity length that is commensurate with waves having both k' and k. The result of the calculation is independent of z_0, the vertical phase of the roll instability with respect to the magnets. The computation is again implemented symbolically using MAPLE.

Figure 10 shows that the magnetic field stabilizes the roll perturbations. The stabilization is strongest if the magnets are far apart (low k), whence the field lines tend to be axial for large sections of the channel. The effect goes to zero as the magnets in the stack are much closer together than the most unstable wavelength ($\sim 2d$) so that the field effects wiggle back and forth many times in one vertical cell height of the instability. There is a small twist in the curve when $k \sim k'$ that is probably experimentally insignificant. For the laboratory parameters given in (16) $\tau MsB_i/\nu\rho_0 = 0.75$. A laboratory realization with $k = 2.5$ should then show a stabilization of about 10% of critical. The parameter c_3 does not vary substantially with k'. For example, if $k = 2.5$ then c_3 varies from 0.137 at $k' = 2$ down to 0.130 at $k' = 5$. The magnetic viscosity will have little influence on wavenumber selection.

6. Conclusions and discussion

We have considered alterations to the basic linear velocity profile of rotating channel flow in a magnetic fluid. These arise because the (constant) vorticity of the channel flow interacts with the magnetic field imposed by the vertical stack of magnets (figure 1) to produce a magnetic moment in the suspended particles that is no longer aligned with the imposed field. This leads to a body force that generates both an x-independent correction $V(x)$, as well as a wavy correction $V(x, z) \propto V_1(x)\cos(2kz)$, where k is the vertical wavenumber of the magnet stack. The wavy correction is

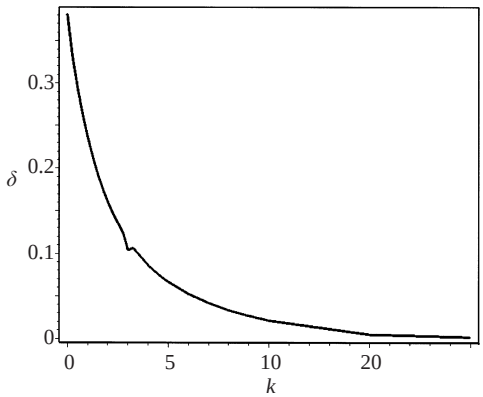

FIGURE 10. Coefficient $c_3(k)$ of the linear instability problem for the gravest instability mode having $k' = 3.117$, $Q_c = -1708$. See equation (33).

resonant whenever $Q = (1 + Ro)/E^2$ is an eigenvalue of the linear stability problem for two-dimensional rotating plane Couette flow modes with vertical wavenumber $k' = 2k$. A weakly nonlinear analysis shows that there can be either one or two stable finite-amplitude states in these cases. For practical laboratory parameter values all the corrections to the basic plane Couette flow are pretty small (a few per cent or less). Under very low rotation, it may be possible to observe the z-dependent basic flow modification.

The effects of 'magnetic viscosity' on the flow instability problem were studied by perturbation analysis. The stabilization is not large, but at 10% or so, it probably measurable for characteristic laboratory parameters. This result, for a fairly complicated magnetic field distribution, is in the same range as previous numerical estimates showing weak stabilization for spatially uniform fields.

The magnet stack approach to generating a large lateral buoyancy effect in magnetic fluids appears plausible in that significant non-Newtonian effects are not anticipated. Another important issue, when considering a 'stratified shear flow' experiment using ferromangetic buoyancy, is the effect of small vertical non-uniformities in $|B|$, with the resulting $\boldsymbol{g}_l = g_1(x)\hat{x} + \boldsymbol{g}_2(x, z)$. The second acceleration, though conservative, may excite more significant waves, when there is a lateral density (or temperature) stratification, than those found here. Such effects are under consideration.

This research was funded by the NASA program in microgravity sciences, through grant NAG-3-2402 to the University of Colorado. I thank Dr Dan Ohlsen for providing figure 3.

Appendix A. Perturbation magnetization and field intensity

In expanding the right-hand side of (1a) we write

$$\boldsymbol{B} = \boldsymbol{B}_0 + \boldsymbol{B}', \quad \boldsymbol{H} = \boldsymbol{H}_0 + \boldsymbol{H}', \quad \boldsymbol{M} = \boldsymbol{M}_0 + \boldsymbol{M}', \tag{A 1}$$

where the primed quantities are the small perturbation. The accelerations we are interested in then appear as

$$\boldsymbol{M} \cdot \nabla \boldsymbol{H} = \boldsymbol{M}_0 \cdot \nabla \boldsymbol{H}_0 + \boldsymbol{M}' \cdot \nabla \boldsymbol{H}_0 + \boldsymbol{M}_0 \cdot \nabla \boldsymbol{H}' + O(\boldsymbol{M}' \cdot \boldsymbol{H}'/d), \tag{A 2}$$

where the last term on the right-hand side of (1*a*) expands similarly. Because of (8), the magnetization $\boldsymbol{M}_0$ due to the basic field intensity $\boldsymbol{H}_0$ has magnitude $\boldsymbol{M}_s$ (assumed greater than $\chi\boldsymbol{H}_0$ here) and is oriented along $\boldsymbol{H}_0 = \boldsymbol{B}_0/\mu_0$. Thus, the first term on the right-hand side of (A 2) may be absorbed into the pressure. The second term is calculated using (10).

Turning to the third term, the expansion of Maxwell's equations gives $\boldsymbol{H}' = \boldsymbol{B}'/\mu_0 - \boldsymbol{M}'$. Since $\nabla \times \boldsymbol{H}' = 0$ and $\nabla\cdot\boldsymbol{H}' = -\nabla\cdot\boldsymbol{M}'$, we have $\boldsymbol{H}' = \nabla\Phi'$, and $\nabla^2\Phi' = -\nabla\cdot\boldsymbol{M}'$. For the basic-state correction problem, $\boldsymbol{M}' = M(x,z)\hat{y}$, and thus the magnetization deviation has no divergence. In addition to solving the interior problem, all magnetic boundary conditions on the side of the ferrofluid channel are also satisfied by taking $\boldsymbol{H}' = 0$. For the linear instability problem, $\boldsymbol{M}'$ is a general vector proportional to the amplitude of the instability. However, it is clear from the above that $\boldsymbol{H}'$ will be of order $\boldsymbol{M}'$. Thus, the ratio of the third term on the right-hand side of (A 2) to the second will be of order $M_0M'/M'H_0 \approx M_s/H_0$ at worst. Since $M_s \ll H_0$, the dominant dynamically significant term on the right-hand side of (A 2) is just the second one.

Appendix B. The equivalent Taylor–Couette problem

The rotating Couette flow problem considered here is asymptotically equivalent to the cylindrical Taylor–Couette problem when the latter has a small gap compared to the inner radius, and when the two rotation rates are nearly equal. In the cylindrical case, let the inner and outer rotation rates be Ω, and $\Omega + \Delta\Omega$, respectively, with $\Delta\Omega/\Omega \ll 1$. Let the inner radius be R and the gap-width be $d \ll R$. The parametric correspondence is then $E = Ta^{-1/2}$, $Ro = \Delta\Omega R/2\Omega d$, $Q = (1 + \Delta\Omega R/2\Omega d)Ta$.

REFERENCES

Bashtovoy, V. G., Berkovsky, B. M. & Vislovich, A. N. 1988 *Introduction to Thermomechanics of Magnetic Fluids*. Springer.

Hart, J. E. 1972 Instability and secondary motion in a rotating channel flow. *J. Fluid Mech.* **45**, 341–351.

Hart, J. E., Glatzmaier, G. A. & Toomre, J. 1986 Space-laboratory and numerical simulations of thermal convection in a rotating hemispherical shell with radial gravity. *J. Fluid Mech.* **173**, 519–544.

Holderied, M., Schwab, L. & Stierstadt, K. 1988 Rotational viscosity of ferrofluids and the Taylor instability in a magnetic field. *J. Phys. Condensed Matter* **70**, 431–433.

Hubbard, J. B. & Stiles, P. J. 1986 Hydrodynamics of magnetic and dielectric colloidal dispersions. *J. Chem. Phys.* **84**, 6955–6968.

Johnston, J. P., Halleen, R. M. & Lezius, D. K. 1972 Effects of spanwise rotation on the structure of two-dimensional fully developed turbulent channel flow. *J. Fluid Mech.* **56**, 531–557.

Kristoffersen, R. & Andersson, H. I. 1993 Direct simulations of low-Reynolds-number turbulent flow in a rotating channel. *J. Fluid Mech.* **256**, 163–197.

Kropp, M. & Busse, F. H. 1991 Thermal convection in differentially rotating systems. *Geophys. Astrophys. Fluid Dyn.* **61**, 127–148.

Matthews, P. & Cox, S. 1997 Linear stability of rotating convection in an imposed shear flow. *J. Fluid Mech.* **350**, 271–293.

Niklas, M. 1987 Influence of magnetic fields on Taylor vortex formation in magnetic fluids. *J. Phys. Condensed Matter* **68**, 493–501.

Niklas, M., Muller-Krumbhaar, H. & Lucke, M. 1989 Taylor-vortex flow of ferrofluids in the presence of general magnetic fields. *J. Magnetism Magnet. Mat.* **81**, 29–38.

Ohlsen, D. R. & Rhines, P. B. 1997 Laboratory studies of equatorially trapped waves using ferrofluid. *J. Fluid Mech.* **338**, 35–58.

Piomelli, U. & Liu, J. 1995 Large eddy simulation of rotating channel flows using a localized dynamic model. *Phys. Fluids* **7**, 839–848.

Rosensweig, R. E. 1985 *Ferrohydrodynamics*. Cambridge University Press.

Shliomis, M. I. 1972 Effective viscosity of magnetic suspensions. *Sov. Phys. J. Exp. Theor. Phys.* **34**, 1291–1294.

Shliomis, M. I. 1974 Magnetic fluids. *Sov. Phys. Uspekhi*. **17**, 153–169.

Stiles, P. J. & Blennerhassett, P. J. 1993 Stability of cylindrical Couette flow of a radially magnetized ferrofluid in a radial temperature gradient. *J. Magnetism Mag. Mat*. **122**, 207–209.

Stiles, P. J., Kagan, M. & Hubbard, J. B. 1987 On the Couette–Taylor instability in ferrohydrodynamics. *J. Collid Interface Sci*. **120**, 430–438.

Tafti, D. K. & Vanka, S. P. 1991 A numerical study of the effects of spanwise rotating on turbulent channel flow. *Phys. Fluids* **3**, 642–656.

Tagg, R. 1994 The Couette–Taylor problem. *Nonlin. Sci.* **4**, 1–25.